

*Short Note*

# The Vallo di Diano Fault System: New Evidence for an Active Range-Bounding Fault in Southern Italy Using Shallow, High-Resolution Seismic Profiling

by Pier Paolo Bruno,\* Luigi Improta, Antonio Castiello, Fabio Villani, and Paola Montone

**Abstract** Range-bounding normal faults can present significant challenges for seismic exploration. This is the case of the fault system bounding the Vallo di Diano, the largest intermountain basin in the southern Apennines seismic belt. Industry reflection profiles define the large-scale structure of the basin but barely image the shallow fault system due to unfavorable topographic and near-surface conditions along the foothills of the eastern range. We present two high-resolution (HR) wide-aperture profiles recorded at the eastern margin of the basin across unreported scarps that affect Middle–Late Pleistocene alluvial fans and slope debris. The survey is aimed at identifying possible recent faulting across these challenging terrains and at understanding the relationship between shallow structures and the master range-bounding fault at depth. Common depth point processing of wide-aperture reflection data and first-arrival travel-time tomography provide detailed images of the upper 200–300 m and sounding evidence of recent activity along previously unknown splays of the fault system. These splays dissect the Mesozoic limestone bedrock and alluvial-fan sequences, affecting their depositional pattern. Very high resolution  $V_p$  and reflectivity images also give hints of possible coseismic surface faulting in Holocene colluvia. These results have relevant implications for the evaluation of the seismogenic potential of the range-bounding fault system and for seismic hazard assessment of the densely urbanized Vallo di Diano basin.

*Online Material:* Table of acquisition and data processing parameters, and figures showing schematic stratigraphy of the Vallo di Diano basin, restoration of fault displacement along the HR profile, and resolution of the  $P$ -velocity tomographic images for the VHR profile.

## Introduction

Range-bounding normal-fault systems can represent a major seismic hazard in active extensional provinces because they can be potential sources of large ( $M \approx 7$ ) earthquakes (e.g., Basin and Range, Intermountain seismic belt, central Greece, Apennines in Italy; Wallace, 1984; Roberts and Jackson, 1991; Mason, 1996; Cello *et al.*, 2003). Fault systems and related extensional basins are commonly investigated by standard seismic reflection surveying (e.g., Smith and Bruhn, 1984) aimed at reconstructing the basin evolution and at constraining the fault geometry, dimension, and kinematics, which are crucial information to assess seismogenic potential.

However, range-bounding faults can present significant challenges for seismic exploration (Smith and Bruhn, 1984).

The main factors hindering seismic imaging are strong lateral velocity contrasts across steeply dipping faults at the basin edges and unfavorable topographic and near-surface conditions along the range slopes. Here, rapid topographic changes and clastic deposits (slope debris and alluvial fans) can pose significant difficulties for data acquisition and processing. In particular, thick and inhomogeneous clastic covers favor diffraction and scattering phenomena, guided waves, ground-rolls, and static problems, which degrade reflection data. Poor quality and resolution mainly affect the shallow portion of reflection profiles (usually down to 500–1000 m depth) and, consequently, a data gap commonly exists between surface geology and the deep seismic images of

\*Also at Department of Exploration Geophysics, Curtin University, 26 Dick Perry Avenue, Kensington, Western Australia 6151, Australia.

range-bounding faults. This problem can hamper the accurate imaging of the shallow architecture of the fault system that is crucial to link morphostructural and paleoseismological observations to deep faulted structures in the perspective of seismogenic potential estimation.

The data gap can be, in principle, filled by high-resolution (HR) near-surface reflection data (e.g., Dolan and

Pratt, 1997). However, for the aforementioned problems reflection imaging of shallow fault zones in inhomogeneous sediments, such as slope debris and alluvial fans, is a difficult task (Stephenson *et al.*, 1993; Mattson, 2004).

An example of data gap between the surface and the deeper structures is evident in Vallo di Diano, the largest intermountain basin in southern Apennines, one of the

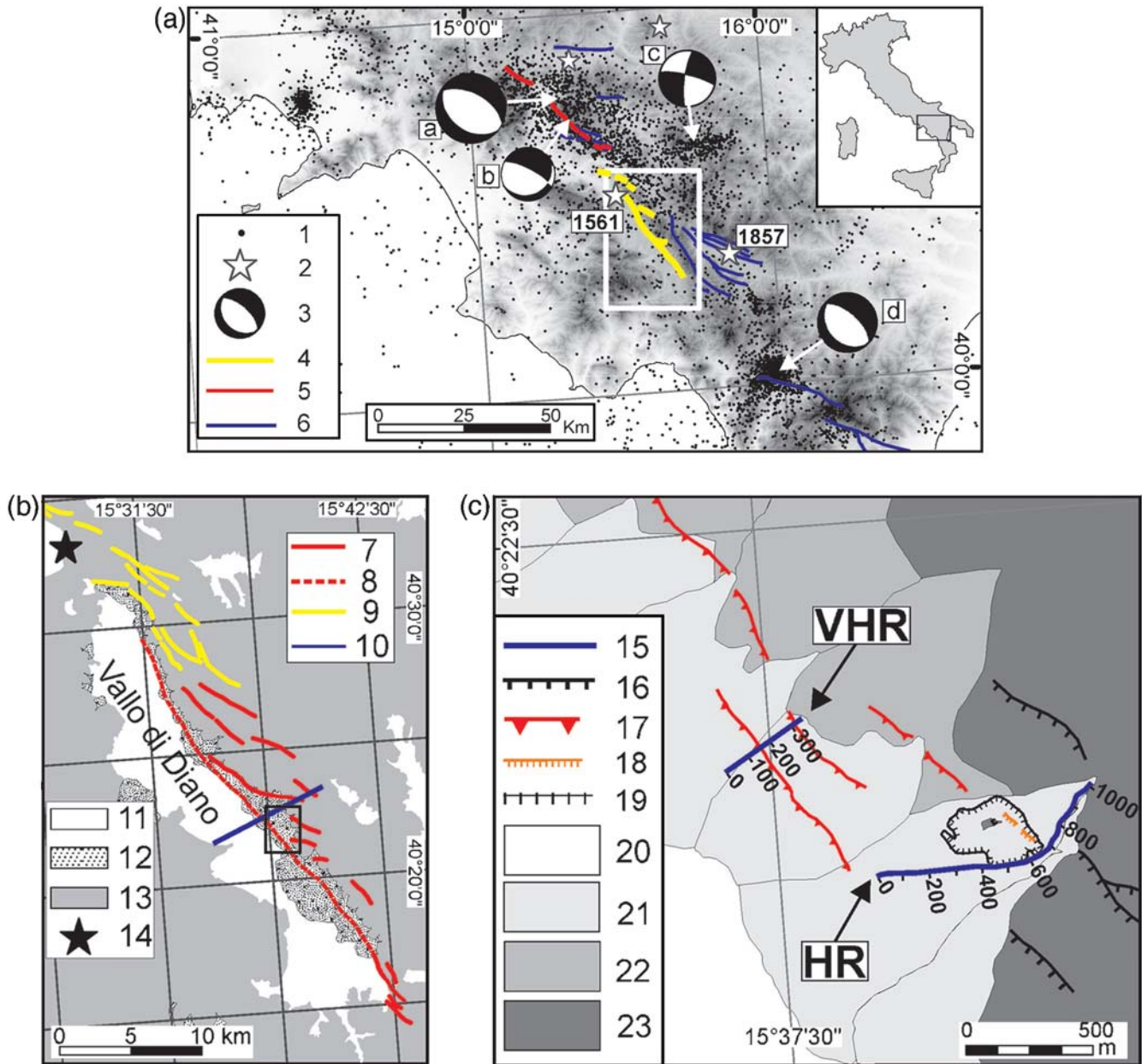


**Figure 1.** (a) Seismicity of the southern Apennines. The white box encloses the area in (b). 1, Crustal seismicity (1981–2002; depth 0–30 km); 2, historical earthquakes ( $M > 6$ ) with the 1561 and 1857 events outlined; 3, focal mechanism of  $M > 5$  events (a, 1980  $M$  6.9; b, 1996  $M$  5.1; c, 1990  $M$  5.7; and d, 1998  $M$  5.6); 4, VDFS; 5, fault scarps of the 1980 Irpinia earthquake; and 6, Quaternary faults. (b) Geological sketch of the Vallo di Diano. The black box encloses the area shown in (c). 7, VDFS in bedrock; 8, VDFS buried; 9, VDFS northern segments active during late Pleistocene–Holocene; 10, location of the industry profile shown in Figure 2c; 11, middle Pleistocene–Holocene lacustrine deposits; 12, alluvial fans and slope breccias (Middle Pleistocene–Holocene); 13, Meso-Cenozoic rocks; and 14, epicenter of the 1561 earthquake. (c) Geological map of the survey area. 15, VHR and HR seismic profiles with CDP positions; 16, normal fault in bedrock; 17, scarp or surface flexures discovered by our morphotectonic surveys; 18, normal faults in Late Pleistocene–Holocene alluvial-fan deposits, discovered by our morphotectonic surveys; 19, quarry; 20, lacustrine deposits (Late Pleistocene–Holocene); 21, alluvial fans (Late Pleistocene–Holocene); 22, alluvial fans and slope breccias (Middle Pleistocene); and 23, Mesozoic carbonates.

central Mediterranean regions with the highest seismic hazard (Fig. 1a). Vallo di Diano is a narrow, 37 km long, northwest-trending structural depression situated ~40 km to the southeast of the 1980  $M_S$  6.9 Irpinia normal-faulting earthquake (Pantosti and Valensise, 1990). It is located in the southern Apennines thrust-belt axial portion that underwent thrusting from Miocene to Late Pliocene (Patacca *et al.*, 1990) and was subsequently subject to Quaternary northeast extension (Cinque *et al.*, 1993). The basin is bordered on both sides by up to 1800 m high ridges made of Mesozoic–Tertiary carbonates, locally covered by Miocene–Pliocene flysch. It is filled in with Early–Middle Pleistocene fluvio-lacustrine deposits (Karner *et al.*, 1999), which grade laterally into Middle Pleistocene–Holocene coalescent fans, forming a complex depositional system along the eastern foothill (a sketch of the stratigraphy of the basin is shown in Fig. S1 available in the electronic edition of *BSSA*). The basin is bounded to the east by a typical range-bounding normal-fault system (Fig. 1b). The system includes northwest-striking, southwest-dipping, extensional and oblique-slip faults for a total length greater than 30 km (Vallo di Diano fault system [VDFS] according to Cello *et al.* [2003]). The VDFS played a primary role in the basin genesis and evolution from Early to Middle Pleistocene, as documented by several seismic industry profiles (Amicucci *et al.*,

2008). However, major uncertainties remain regarding its Late Pleistocene–Holocene activity. While recent deformation (Cello *et al.*, 2003) and probable historical coseismic surface rupturing (Galli *et al.*, 2006) are reported in the literature for the northernmost splays (Fig. 1b), neither surface geology, nor seismic reflection profiles, nor seismicity data yield clues to recent activity for the central and southern sectors of the basin.

Difficulty in finding geomorphic evidence for recent activity is mainly due to thick Late Pleistocene–Holocene alluvial-fan and slope deposits draping most of the central and southern segments of the VDFS at the foothills of the eastern range (Fig. 1b). Industry profiles reveal the large-scale structure of the basin (Fig. 2c), but the shallow, fine-scale imaging of the VDFS is poor along the foothills of the eastern range due to acquisition gaps, a rough topography, thick clastic deposits, and strong lateral velocity contrasts between Mesozoic limestone and continental deposits (Fig. 1b). Consequently, the fault geometry is mostly inferred from the asymmetric pattern of the basin infill (Fig. 2c).

Present-day seismicity contributes minimally to active fault detection because only a scarce and sparse microseismicity characterizes the Vallo di Diano (Fig. 1a). Nonetheless, the high-seismogenic potential of this sector of the Apennines is testified by the 1561 ( $M_e$  6.4) and 1857 ( $M_e$  7) destructive

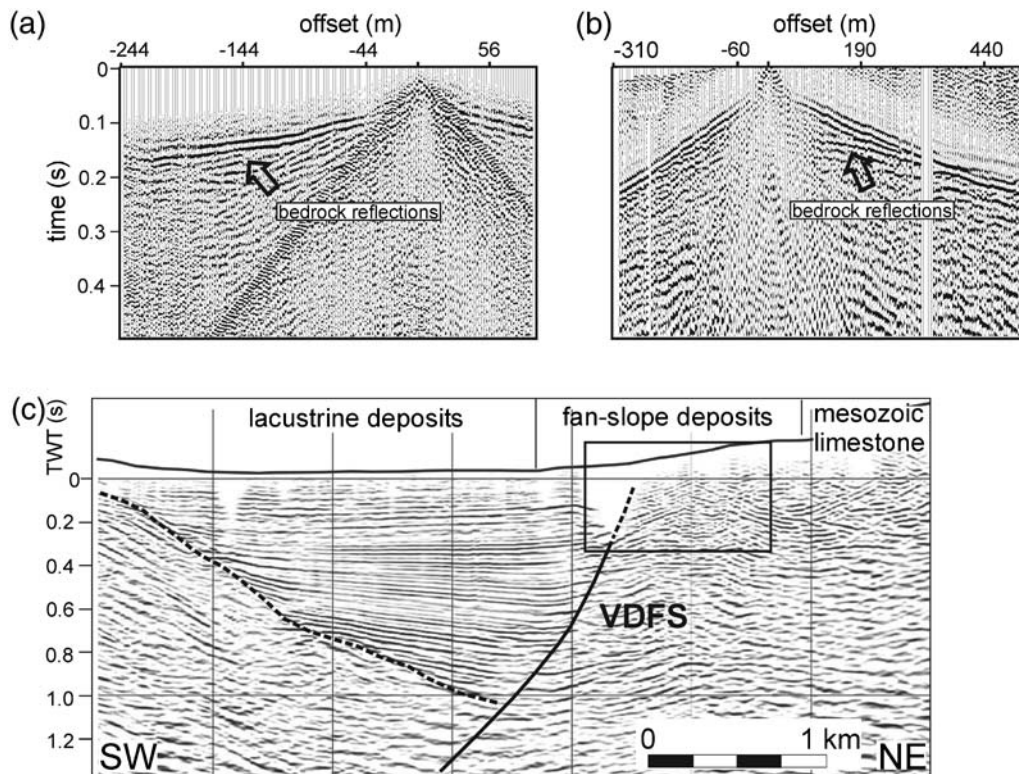


**Figure 2.** (a) Raw shot gather acquired along the VHR profile using a buffalo gun. (b) Raw shot gather acquired along the HR profile using the vibroseis source. The arrows outline the reflected phases. (c) Commercial seismic profile across the Vallo di Diano and VDFS (modified after Amicucci *et al.*, 2008). The dashed line outlines the basin bottom. The box defines the crustal section investigated in this article. Shallow imaging is ineffective along the eastern margin of the basin, preventing the detection of the VDFS.

earthquakes, with macroseismic epicenters located to the north (~5 km) and to the east (~20 km) of the basin, respectively (CPTI Working Group, 2004; Fig. 1a,b).

An important question about the seismogenic potential of the Vallo di Diano range-bounding fault system remains unanswered: is the Holocene activity limited to the VDFS northern splays (e.g., Cello *et al.*, 2003) or does it involve other fault segments? Addressing this issue is crucial, especially after the recognition of previously unknown flexures in the central part of the basin, which suggest recent activity along the VDFS (Castiello *et al.*, 2008). We mapped northwest-trending, 400–900 m long and 0.8–2 m high fault scarps and surface flexures in Late Pleistocene–Holocene alluvial fans, which cover the central sector of the VDFS (Fig. 1b,c).

These new morphotectonic findings provided the motivation for the execution of shallow, HR reflection/refraction surveys. Two profiles were planned to cross the scarps and flexures recognized in recent deposits, with the aim of filling the imaging gap between the surface and the commercial seismic reflection data (Fig. 2c). Our primary objectives were (1) verifying the presence of a fault zone within these strongly inhomogeneous terrains, which can challenge the seismic method's ability to image geologic features (Stephenson *et al.*, 1993; Mattson, 2004), (2) understanding the relationship between shallow faulted structures and the range-bounding fault imaged by industry profiles, and (3) shedding light on the recent evolution of the VDFS. The use of advanced acquisition and processing schemes (e.g., Bruno and Castiello, 2009) allowed us to successfully image this challenging target down to ~300 m depth. Our seismic images provide evidence of recent deformation along previously unknown fault splays of the VDFS. Additionally, very detailed  $V_p$  tomographic and reflectivity images of these splays show hints of faulting in near-surface Holocene deposits.

### The Survey

We adapted the dense wide-aperture acquisition strategy used in hydrocarbon exploration of complex structures (Ravaut *et al.*, 2004) to shallow targets. Dense shots were recorded by a geophones spread with aperture length 3 to 4 times larger than the expected depth of the exploration target. This acquisition geometry differs from typical common midpoint small-aperture reflection surveying as it aims at recording both multifold reflection data spanning a large range of offsets (from small-offset near-vertical reflections to large-offset large-amplitude postcritical reflections) and deep-penetrating refracted waves, which are suitable for first-arrival travel-time tomography. Tomography not only contributes information about the subsurface structure but also provides a good control on the velocity structure that is crucial for improving the reliability of the static corrections and, ultimately, the stacking of shallow reflections (Improta and Bruno, 2007; Bruno and Castiello, 2009).

We collected two HR and very high resolution (VHR) profiles by using a 168 channel acquisition device. Both profiles strike southwest–northeast and run over Holocene colluvial soils, which cover Middle–Upper Pleistocene alluvial-fan deposits and Middle Pleistocene slope breccias (Fig. 1c). The HR profile, located ~3 km to the south of a commercial line (Amicucci *et al.*, 2008; Fig. 1b), was designed to illuminate the first 0.2–0.3 sec two-way travel time (TWT) along the basin edge, which is missing on industry data due to poor data quality and resolution (Fig. 2c). This profile is ~1000 m long and tied at the northeast ending to the exposed Mesozoic limestone, and it was acquired by moving an 835 m long array of receivers, with geophone spacing of 5 m.

The VHR profile specifically targeted the near-surface structure (<100 m depth) across topographic flexures well constrained by leveling profiles. The VHR line is 350 m long and was acquired by a fixed array of receivers, with geophone spacing of 2 m. An effective HR vibrating source manufactured by Industrial Vehicles International (IVI) and named as MINIVIB was used for the HR profile. For the VHR line we preferred a buffalo gun, a weaker and lower frequency source, but more suitable to model the very shallow subsurface with refraction tomography because it allows the collection of very clear first arrivals at small offsets (Fig. 2a,b). Source move up was 10 and 4 m for the HR and VHR profiles, respectively.

Figures 2a,b show two examples of unprocessed common shot gathers (CSGs) for both profiles. Data quality is high, and it varies along the seismic lines, depending on near-surface conditions. The HR line was acquired and processed with a crooked geometry for logistic reasons. Accurate static corrections are crucial to successfully image shallow reflections (Stephenson *et al.*, 1993). Because both profiles cross an area of rugged topography and significant near-surface velocity changes, static corrections played a primary role in our processing. High-precision topographic leveling and the good near-surface velocity control achieved by travel-time tomography allowed accurate tomographic corrections (Zhu *et al.*, 1992). Residual statics were also performed to mitigate short-wavelength static time shifts. Integration of tomographic models and semblance was used to calculate the best stacking velocities (see Table S1, [E](#) available in the electronic edition of *BSSA*, that summarizes the field acquisition parameters and processing steps for both profiles).

Overall, velocities range from 700 to 2000 m/sec in the shallower portion (from 0 to 20–40 m depth) up to 3500 to 4500 m/sec (below 50–250 m depth), where waves propagate within cemented Middle Pleistocene breccia or Mesozoic fractured limestone. For both profiles the estimated vertical/horizontal resolution at the top of the Mesozoic limestone bedrock is ~12/25 m, respectively. Vertical/horizontal resolution increases upward within the alluvial fans up to 3/6 m, respectively.

The first-break picking took advantage of the redundant reciprocity relationships between CSGs, (Morey and Schuster,

1999). First arrivals were handpicked with uncertainties ranging from 2 msec, which is about 1/8 of the dominant period of the first arrivals, to 9 msec. The root mean square picking error was 2.1 msec for the VHR profile (1.42E+4 readings) and 2.7 msec for the HR profile (1.48E+4 readings). First-arrival times for the VHR line were input to a nonlinear, multiscale tomographic algorithm based on a finite-difference eikonal solver. This tomographic technique, specifically designed to investigate complex crustal structures (Improta *et al.*, 2002; Improta and Corciulo, 2006), has been adapted for shallow targets and successfully used to resolve faulted structures (Improta *et al.*, 2003). For the HR profile, travel-time tomography was limited to small-offset first breaks because of the crooked geometry. In this case, we simply estimated the near-surface velocity field required for tomostatics by

means of a standard, less time-consuming iterative-linearized commercial algorithm (Sheehan *et al.*, 2005).

## Results

The HR profile in Figure 3 shows several alluvial-fan sequences with complex morphological patterns. These sequences are separated by clear unconformities and lie above the Mesozoic limestone bedrock, which is generally reflection free (*a* in Fig. 3b). The top of the bedrock is imaged as a high-amplitude, low-frequency seismic unconformity, and it is truncated by a set of generally southwest-dipping high-angle faults. A major fault zone, characterized by a complex reflection configuration, extends between positions 280 and 380 m (*fz* in Fig. 3b). Normal faulting is responsible for noticeable back-tilt and vertical throw of

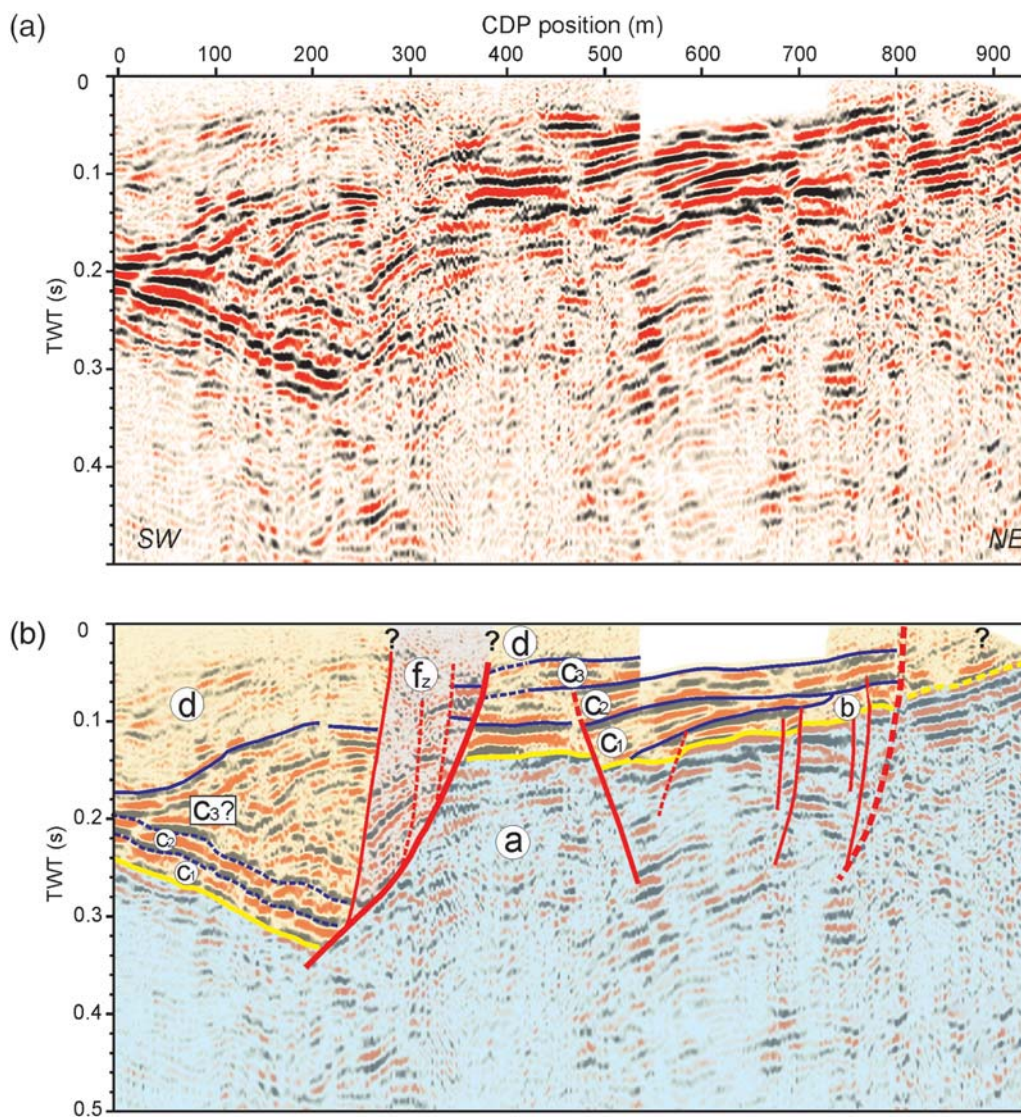


**Figure 3.** (a) HR seismic reflection section and (b) interpretation. Symbols: *a*, Mesozoic carbonates; *b*, *c*, *c*<sub>1</sub>, *c*<sub>2</sub>, *c*<sub>3</sub>, and *d*, Quaternary continental sequences; *f*<sub>z</sub>, fault zone; yellow line, top of the bedrock; blue line, main unconformities; red line, faults; and dashed line, uncertain fault. The acquisition gap between 540 and 730 m corresponds to out of plane CDPs removal across the quarry due to crooked line geometry (see Fig. 1c).

the limestone bedrock (about 0.20 sec TWT, corresponding to  $\sim 170$  m;  $V_P = 1700$  m/sec) and of at least two Middle Pleistocene sequences ( $c_1$  and  $c_2$  in Fig. 3b; see also Fig. S2, ⑤ available in the electronic edition of *BSSA*, that shows restoration of fault displacement around position 380 m). An antithetic fault, at position 500 m, partially controls deposition of layers  $c_1$  and  $c_2$ , but it is in turn truncated by a shallower unconformity ( $c_3$ ) at 0.06 sec. It is noteworthy that we reported at the bottom of the quarry a northeast-dipping normal-fault plane in bedrock (sealed by alluvial-fan deposits) (Fig. 1c) that could be related to the fault at position 500 m. Moving toward the northeast, minor fault splays displace the oldest continental sequence between 600 and 800 m ( $b$  in Fig. 3b) and are sealed by subsequent alluvial-fan sediments ( $c_1$  in Fig. 3b). At position 800 m, an abrupt change in polarity and a slight change of dip of the reflectors across a disrupted area, visible between 0.05 and

0.2 sec TWT, may suggest the presence of a high-angle southwest-dipping fault. However, the lack of correlative reflectors (such as the top of limestone bedrock) on both sides of the hypothesized fault makes fault detection ambiguous and hampers assessment of its throw and kinematics.

Interpretation of the VHR profile relies on the complementary information provided by seismic tomography and common depth point (CDP) stack section. Tomographic velocity models at different scales are shown in Figures 4a,b. We discuss a long-wavelength model (34 m horizontal and 24 m vertical node spacing, Fig. 4a) and a short-wavelength model (17 m horizontal and 11 m vertical node spacing, Fig. 4b) characterized by a resolution depth of  $\sim 100$  and  $\sim 40$  m, respectively (see the results of resolution tests in Fig. S3 ⑤ available in the electronic edition of *BSSA*). The most noticeable feature of the long-wavelength model is the abrupt southwest deepening of a prominent high- $V_P$  region (3500–4500 m/sec) around 250 m distance (Fig. 4a). This feature is outlined by the abrupt change in depth of the 3400–3800 m/sec contours, showing a vertical separation of  $\sim 50$  m, and it is accompanied upward by a gradual southwest thickening of the region with  $V_P = 1800$ –3000 m/sec. This region is bounded to the southwest by a high  $V_P$  bump, with velocity  $\sim 3000$  m/sec, located between 50 and 100 m. In the short-wavelength shallow model (Fig. 4b), low  $V_P$  regions bound high-velocity ( $V_P > 2500$  m/sec) bodies positioned around 50, 125, and 225 m distance between 15 and 25 m deep. At position 280 m, a rapid southwest deepening of the 2600–3400 m/sec contours, showing a vertical separation of  $\sim 20$  m, delineates a shallow secondary step at  $\sim 20$  m depth (Fig. 4b). This step, which is located 30 m to the northeast of the main lateral velocity change in Figure 4a, is associated with southwest thickening of low  $V_P$  ( $< 1000$  m/sec) near-surface colluvia and spatially correlates with a surface flexure at 300 m (Fig. 4b). Low  $V_P$  near-surface colluvia also thicken to the southwest of a clear surface scarp at position 150 m (Fig. 4b).

The VHR reflection profile shown in Figure 4c is dominated by a high-amplitude, low-frequency series of reflectors between 0.05 and 0.25 sec TWT. The attributes of this reflective package are very similar to those related to the top of carbonates on the HR profile. This association is also supported by the overall agreement between this reflector and the geometry of the high  $V_P$  region, with velocities exceeding 4000 m/sec, which we interpret as the Mesozoic carbonate rocks (Fig. 4a,c). In Figure 4c, two fault segments dissect the top of the carbonates and the upper sequence, possibly reaching the very near surface at about 260 and 300 m. The position of these steps is consistent with the southwest drop in the high-velocity region imaged by seismic tomography. Cumulative vertical throw is at least  $\sim 0.07$  sec (corresponding to  $\sim 80$  m of vertical separation, using a mean tomographic velocity of 2200 m/sec). An antithetic fault at position 75 m dissects the top of the carbonates. In this region, the carbonate bedrock is too deep to be properly resolved by tomography, but there are hints of possible fault disturbance

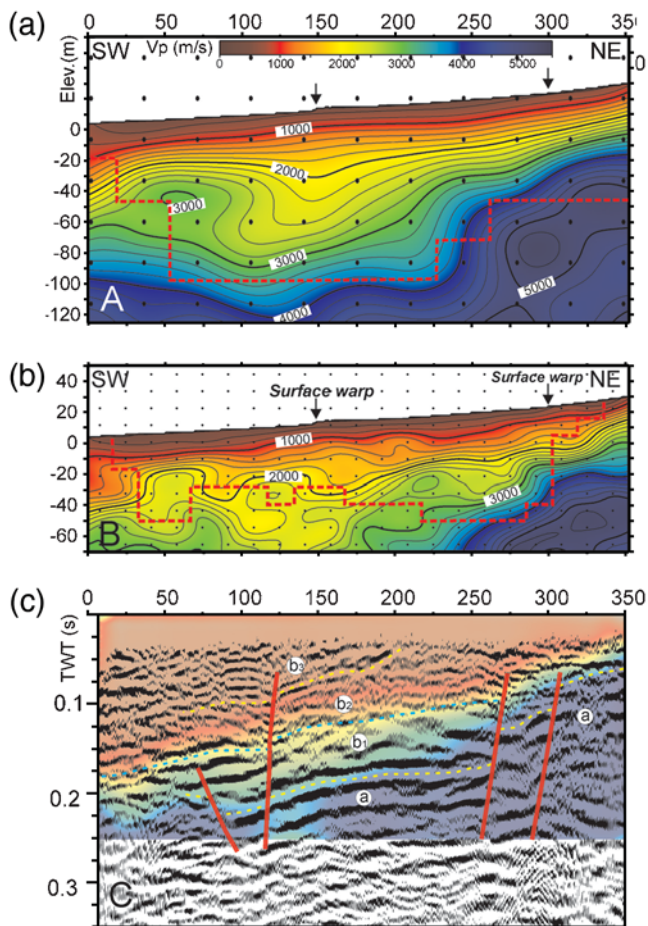


**Figure 4.** (a) Long-wavelength  $V_P$  tomogram for the VHR profile (34 m horizontal and 24 m vertical node spacing). The red dashed line indicates the resolution depth, the black circles depict velocity nodes, and the arrows denote scarps. (b) Small-wavelength  $V_P$  tomogram (17 m horizontal and 11 m vertical node spacing). (c) Seismic reflection section superimposed on the long-wavelength tomogram converted from depth to TWT and referenced to the datum. Symbols:  $a$ , Mesozoic carbonates;  $b_1$ ,  $b_2$ , and  $b_3$ , Quaternary alluvial-fan sequences.

in the long-wavelength velocity model (see the pattern of the contours around 4000 m/sec superimposed to the stack section). The presence of an antithetic normal fault could also explain the rise of the high  $V_p$  ( $\sim 3000$  m/sec) body on the southwest side of the model in Figure 4a. Finally, a further fault splay seems to dissect the upper reflectors at position 125 m.

### Discussion

Comparison between industry (Fig. 2c) and our HR reflection profile (Fig. 3) highlights a remarkable improvement in shallow imaging of the VDFS. The basin-bounding master fault, detected at depth by the commercial profile, is barely visible above 0.4 sec TWT. Our HR profile indicates that the deep master fault links to a shallow deformation zone, at least 800 m wide, developed along the foothills of the eastern range. Deformation, which seems localized at depth on the master fault, is partitioned upward through a complex system of synthetic and antithetic faults, which displace and control the deposition of Middle and Late Pleistocene alluvial-fan sequences and slope debris up to 300 m thick. Although shallow imaging of faulted structures in thick, inhomogeneous, clastic deposits is difficult, our acquisition/processing strategy has led to detailed structural images of the shallow VDFS, by which an improved understanding of the recent evolution has been achieved.

Both profiles provide sounding evidence for recent activity along unknown splays of the VDFS. The HR profile reveals truncations of near-surface reflectors and a main fault zone at position 280–380 m. Prolonged synsedimentary activity is documented by the dramatic thickening of the hanging-wall infill ( $c3?$  and  $d$  in Fig. 3b). Restoration of fault displacement at position 380 m indicates that pure normal kinematics of this fault is the most plausible (see Fig. S2 ⑤ available in the electronic edition of *BSSA*). Moreover it suggests that sequences  $c1$  and  $c2$  predate faulting, thus indicating a probable Middle Pleistocene age for normal-faulting inception. The thick wedge ( $c3?$  in Fig. 3b) is characterized by a sigmoid progradational pattern, consisting of thicker foresets downlapping the top of the carbonates and featuring both top-set and bottom-set thinner strata; this configuration mirrors a classical Gilbert-type delta, which is typical of continental fans flowing into fluviolacustrine basins. The overall antiformal shape of this growth structure may be related to the progressive back-tilting and deformation of foresets inside  $c3?$ , and it could have enhanced clinostratification of the upper layers ( $d$  in Fig. 3b). Following Cello *et al.* (2003), who stress the importance of transtensional and strike-slip tectonics in this area during Early–Middle Pleistocene, a different interpretation of the domelike upper bound of the  $c3?$  body might be proposed. Strike-slip tectonics may have promoted localized block rotation in the hanging wall (see the variable dip of layers in the fault zone  $fz$  between 300 m and 400 m in Fig. 3), while local compression may have been caused by along-strike

fault-bending, which cannot be recovered on our seismic line.

Faulting in the very near surface at position 380 m is uncertain due to low resolution above 0.04 sec TWT.

Nevertheless, a subtle warping of the shallowest hanging-wall reflectors within unit  $d$  may suggest the ongoing fault activity causing drag folding.

The HR profile also shows hints of faulting at location 800 m. Normal faulting at this position is consistent with field data: northwest-trending bedrock fault scarps are located just to the south of the profile, and, more importantly, fault splays dissecting Late Pleistocene–Holocene fan deposits have been recently recognized in the quarry (Castiello *et al.*, 2008; see Fig. 1c).

On the VHR profile, the main indication of very recent deformation along southwest-dipping normal faults comes from the velocity models that detect, between 250 and 280 m, two steps in the carbonate bedrock and a concurrent southwest thickening of near-surface Holocene colluvia in the fault hanging wall (Fig. 4a,b). The seismic reflection section supports our interpretation by showing southwest-dipping normal faults and a rapid southwest deepening of the carbonate bedrock between 260 and 300 m (Fig. 4c). Seismic tomography and reflection data also yield a comparable estimate of the cumulative vertical throw in this portion of the section ( $\sim 70$  and  $\sim 80$  m, respectively). Truncation/warping of near-surface reflectors (up to  $\sim 0.075$  sec TWT) are additional indications of very recent deformation. It is noteworthy that all these signatures are located just in front of the surface flexure recognized in the field at  $\sim 300$  m and affecting the Late Pleistocene–Holocene alluvial-fan sediments and colluvia. On the other hand, the flexure at 150 m is more ambiguous, as both the reflectivity and the  $V_p$  images contain only hints of shallow faulting, which are warped/truncated weak events up to  $\sim 0.05$  sec TWT (Fig. 4c) and a southwest-thickening of Holocene colluvia ( $V_p < 1000$  m/sec; Fig. 4b).

Following the results of multidisciplinary surveys carried out on active basin-bounding normal faults in the western United States (Morey and Schuster, 1999; Sheley *et al.*, 2003; Mattson, 2004), we could tentatively infer recent coseismic surface faulting from the VHR profile. Indeed, as the cited authors point out by comparing shallow tomography and reflection profiling with paleoseismological trenches, the coexistence of (1) steps in high  $V_p$  bodies, (2) thickening of low  $V_p$  colluvia in the hanging wall, and (3) deformation of reflectors in the very near surface can be diagnostic of recent coseismic surface-faulting episodes.

Unfortunately, correlation between reflectivity features of the HR and VHR profiles is unfeasible. The main factors hindering a reliable and accurate comparison are the following: (1) the two profiles, which were traced basing on logistic constraints, do not overlap; (2) different sources were used; and (3) the VDFS has a considerable complexity at shallow structural levels, with prominent along-strike variations, which make the correlation difficult, even over distances

shorter than 1 km. Nevertheless, we tentatively propose that the fault zone at position 280–380 m on the HR profile could correlate with the two fault segments on the northeast side of the VHR profile. The resulting N140°–150° strike is consistent with the trend of the surface flexures and faults affecting Late Pleistocene–Holocene fans discovered by our morphotectonic surveys (Castiello *et al.*, 2008; Fig. 1c). This interpretation implies that fault throw decreases northwestward, which is plausible if the fault edge is located to the northwest.

### Conclusions

The dense wide-aperture seismic profiles yield the first documentation of recent and probable coseismic, normal faulting in alluvial fans and slope debris covering the central segment of the VDFS, along the eastern margin of the basin. Shallow faults merge at depth to the range-bounding master fault inferred by industry profiles and appear spatially correlated with surface flexure affecting Holocene colluvia (Fig. 4). Thus, our survey reveals that recent activity is not limited to the northern splays of VDFS, as reported in previous structural studies (e.g., Cello *et al.*, 2003) but also involves the central sector of the basin. This result bears significant implications for the evaluation of the seismogenic potential of VDFS and in general for seismic hazard assessment of the densely populated Vallo di Diano basin (70,000 inhabitants).

Historical and instrumental seismicity catalogs (CPTI Working Group, 2004, Castello *et al.*, 2006, Valoroso *et al.*, 2009) show that the central–southern sector of the basin is not associated with historical earthquakes nor is releasing seismicity. As a working hypothesis, based on the results of our survey and on geological and geophysical data available, we propose that the central segment of VDFS is a locked seismogenic structure that is building up tectonic stress.

At a more general scale, this article proves the efficiency of the dense wide-aperture profiling, for the shallow, HR exploration of range-bounding faults.

### Data and Resources

All the seismic data processed in this article were collected by the authors during active seismic experiments. The remaining geologic and geophysical data shown in this article came from published sources listed in the references.

### Acknowledgments

We thank Diane I. Doser and an anonymous reviewer whose comments improved the manuscript. We are grateful to Dario De Rosa, Vincenzo Di Fiore, Simona Pierdominici, Michele Punzo, and Francesco Varriale for their valuable help during field work. The authors would like to acknowledge Paolo Gasparini and Roberto Muti of Analisi e Monitoraggio del Rischio Ambientale s.c.a.r.l. for help in coordinating the data acquisition with the MINIVIB. The collaboration of Antonio Rapolla and Consorzio inter-Universitario per la previsione e prevenzione dei Grandi Rischi, in providing part of the instrumentation, is kindly acknowledged. This work was carried

out in the frame of the MIUR-FIRB Project Research and Development of New Technologies for Protection and Defence Territory from Natural Risks (WP-C3, coordinator Paola Montone). Finally, we thank Antonio Rovelli and Enzo Boschi for their continuous encouragements.

### References

- Amicucci, L., M. R. Barchi., P. Montone, and N. Rubiliani (2008). The Vallo di Diano and Auletta extensional basins in the southern Apennines (Italy): A simple model for a complex setting, *Terra Nova* **20**, 475–482, doi [10.1111/j.1365-3121.2008.00841.x](https://doi.org/10.1111/j.1365-3121.2008.00841.x).
- Bruno, P. P., and A. Castiello (2009). High-resolution onshore seismic imaging of complex volcanic structures: An example from Vulcano Island (Italy), *J. Geophys. Res.* **114**, B12303, doi [10.1029/2008JB005998](https://doi.org/10.1029/2008JB005998).
- Castello, B., G. Selvaggi, C. Chiarabba, and A. Amato (2006). CSI Catalogo della sismicità italiana 1981–2002, versione 1.1, INGV-CNT, Roma, available at <http://csi.rm.ingv.it/> (last accessed November 2009).
- Castiello, A., F. Villani, P. P. Bruno, L. Improta, A. D. De Rosa, V. Di Fiore, M. Punzo, F. Varriale, P. Montone, S. Pierdominici, and A. Rapolla (2008). The Vallo di Diano range-bounding fault system (southern Italy): New evidence of recent activity from high-resolution seismic profiling (Abstract S11C-1750), *Eos Trans. AGU* **89**, no. 53 (Fall Meet. Suppl.), S11C-1750.
- Cello, G., E. Tondi, L. Micarelli, and L. Mattioni (2003). Active tectonics and earthquake sources in the epicentral area of the 1857 Basilicata earthquake (southern Italy), *J. Geodyn.* **36**, 37–50, doi [10.1016/S0264-3707\(03\)00037-1](https://doi.org/10.1016/S0264-3707(03)00037-1).
- Cinque, A., E. Patacca, P. Scandone, and M. Tozzi (1993). Quaternary kinematic evolution of the southern Apennines. Relationships between surface geological features and deep lithospheric structures, *Ann. Geofisc.* **36**, 249–260.
- CPTI Working Group (2004). *Catalogo Parametrico dei Terremoti Italiani*, v. 2004 (CPTI04), INGV, Bologna, available at <http://emidius.mi.ingv.it/CPTI04/> (last accessed December 2006).
- Dolan, J. F., and T. L. Pratt (1997). High-resolution seismic reflection profiling of the Santa Monica fault zone, west Los Angeles, California, *Geophys. Res. Lett.* **24**, no. 16, 2051–2054.
- Galli, P., V. Bosi, S. Piscitelli, A. Giocoli, and V. Scionti (2006). Late Holocene earthquakes in southern Apennine; Paleoseismology of the Caggiano fault, *Geol. Rundsch.* **95**, no. 5, 855–870.
- Improta, L., and P. P. Bruno (2007). Combining seismic reflection with multifold wide-aperture profiling: An effective strategy for high-resolution shallow imaging of active faults, *Geophys. Res. Lett.* **34**, L20310, doi [10.1029/2007GL031893](https://doi.org/10.1029/2007GL031893).
- Improta, L., and M. Corciulo (2006). Controlled source non-linear tomography: A powerful tool to constrain tectonic models of the southern Apennines orogenic wedge, Italy, *Geology* **34**, no. 11, 941–944.
- Improta, L., A. Zollo, P. P. Bruno, A. Herrero, and F. Villani (2003). High-resolution seismic tomography across the 1980 ( $M_s$  6.9) southern Italy earthquake fault scarp, *Geophys. Res. Lett.* **30**, no. 10, 1494–1498.
- Improta, L., A. Zollo, A. Herrero, M. R. Frattini, J. Virieux, and P. Dell'Aversana (2002). Seismic imaging of complex structures by non-linear traveltimes inversion of dense wide-angle data: Application to a thrust belt, *Geophys. J. Int.* **151**, 264–278.
- Karner, D. D., E. Juvigne, L. Brancaccio, A. Cinque, E. Russo Ermolli, N. Santangelo, S. Bernasconi, and L. Lirer (1999). A potential early middle Pleistocene tephrostratotype for the Mediterranean basin: The Vallo di Diano, Campania, Italy, *Global and Planetary Change* **21**, 1–15.
- Mason, D. B. (1996). Earthquake magnitude potential of the Intermountain seismic belt, USA, from surface-parameter scaling of late Quaternary faults, *Bull. Seismol. Soc. Am.* **86**, no. 5, 1487–1506.
- Mattson, A. (2004). Tomographic imaging of late Quaternary faulting, Quairrh Mountains, Utah, *J. Geophys. Res.* **109**, B11310, doi [10.1029/2004JB003159](https://doi.org/10.1029/2004JB003159).

- Morey, D., and G. T. Schuster (1999). Palaeoseismicity of the Oquirrh fault, Utah from shallow seismic tomography, *Geophys. J. Int.* **138**, no. 1, 25–35.
- Pantosti, D., and G. Valensise (1990). Faulting mechanism and complexity of the November 23, (1980), Campania-Lucania earthquake, inferred from surface observations, *J. Geophys. Res.* **95**, no. 15, 319–341.
- Patacca, E., R. Sartori, and P. Scandone (1990). Tyrrhenian basin and Apenninic arcs: Kinematic relations since Late Tortonian times, *Mem. Soc. Geol. Ital.* **45**, 425–451.
- Ravaut, C., S. Operto, L. Improta, J. Virieux, A. Herrero, and P. Dell'Aversana (2004). Multiscale imaging of complex structures from multifold wide-aperture seismic data by frequency-domain full-waveform tomography: Application to a thrust belt, *Geophys. J. Int.* **159**, 1032–1056.
- Roberts, S., and J. Jackson (1991). Active normal faulting in central Greece: An overview, *Geol. Soc. London, Spec. Publ.* **56**, 125–142.
- Sheehan, J. R., W. E. Doll, and W. A. Mandell (2005). An evaluation of methods and available software for seismic refraction tomography analysis, *J. Environ. Eng. Geophys.* **10**, 21–34.
- Sheley, D., T. Crosby, M. Zhou, J. Giacomini, J. Yu, R. He, and T. Schuster (2003). 2-D seismic trenching of colluvial wedges and faults, *Tectonophysics* **361**, no. 1–4, 51–69.
- Smith, R. B., and R. L. Bruhn (1984). Intraplate extensional tectonics of the Eastern Basin-Range: Inferences on structural style from seismic reflection data, regional tectonics, and thermal-mechanical models of brittle-ductile deformation, *J. Geophys. Res.* **89**, no. B7, 5733–5762.
- Stephenson, W. J., R. B. Smith, and J. R. Pelton (1993). A high-resolution seismic reflection and gravity survey of Quaternary deformation across the Wasatch fault, Utah, *J. Geophys. Res.* **98**, no. B5, 8211–8223.
- Valoroso, L., L. Improta, L. Chiaraluce, R. Di Stefano, L. Ferranti, A. Govoni, and C. Chiarabba (2009). Active faults and induced seismicity in the Val d'Agri region (southern Apennines, Italy), *Geophys. J. Int.* **178**, 488–501, doi [10.1111/j.1365-246X.2009.04166.x](https://doi.org/10.1111/j.1365-246X.2009.04166.x).
- Wallace, R. E. (1984). Pattern and timing of late Quaternary faulting in the Great Basin province and relation to some regional tectonic features, *J. Geophys. Res.* **89**, 5763–5769.
- Zhu, X., D. P. Sixta, and B. G. Angstman (1992). Tomo-static: Turning ray tomography and static corrections, *The Leading Edge* **11**, 15–23.

Istituto Nazionale di Geofisica e Vulcanologia  
Osservatorio Vesuviano  
Via Diocleziano, 328  
80124, Napoli, Italy  
(P.P.B.)

Istituto Nazionale di Geofisica e Vulcanologia, Sismologia e Tettonofisica  
Via di Vigna Murata 605  
00143, Roma, Italy  
improta@ingv.it  
(L.I., A.C., F.V., P.M.)

Manuscript received 4 August 2009